International Journal of Pharmaceutics 661 (2024) 124389

Contents lists available at ScienceDirect

International Journal of Pharmaceutics

journal homepage: www.elsevier.com/locate/ijpharm

Targetable domains for the design of peptide-dendrimer inhibitors of SARS-CoV-2

Rosa Bellavita [a,1], Speranza Esposito [b,c,1], Simone Braccia [a], Laura Madrid [d], Paula Ortega [d,e,f], Gabriella D'Auria [a], Federica Zarrilli [b,c], Felice Amato [b,c], Stefania Galdiero [a], Javier de la Mata [d,e,f,*], Lucia Falcigno [a,*], Annarita Falanga [g,*]

[a] Department of Pharmacy, School of Medicine, University of Naples 'Federico II', Via Domenico Montesano 49, 80131 Naples, Italy
[b] Dipartimento di Medicina Molecolare e Biotecnologie Mediche, Università di Napoli Federico II, 80131 Naples, Italy
[c] CEINGE Biotecnologie Avanzate Franco Salvatore, Scarl, 80131 Naples, Italy
[d] Universidad de Alcalá, Department of Organic and Inorganic Chemistry, Faculty of Sciences, and Research Institute in Chemistry "Andrés M. del Río" (IQAR), Italy
[e] CIBER de Bioingeniería, Biomateriales y Nanomedicina, Instituto de Salud Carlos III, 28801 Alcalá de Henares, Spain
[f] Institute Ramón y Cajal for Health Research (IRYCIS), 28034 Madrid, Spain
[g] Department of Agricultural Science, University of Naples 'Federico II', Via Università 100, Portici, 80055 Portici, Italy

ARTICLE INFO

Keywords:
SARS-CoV-2
Peptides
Inhibitors
Antiviral
Dendrimers

ABSTRACT

We have recently witnessed that considerable progresses have been made in the rapid detection and appropriate treatments of COVID-19, but still this virus remains one of the main targets of world research. Based on the knowledge of the complex mechanism of viral infection we designed peptide-dendrimer inhibitors of SARS-CoV-2with the aim to block cell infection through interfering with the host-pathogen interactions. We used two different strategies: i) the first one aims at hindering the virus anchorage to the human cell; ii) the second −strategy points to interfere with the mechanism of virus-cell membrane fusion.

We propose the use of different nanosized carriers, formed by several carbosilane dendritic wedges to deliver two different peptides designed to inhibit host interaction or virus entry. The antiviral activity of the peptide-dendrimers, as well as of free peptides and free dendrimers was evaluated through the use of SARS-CoV-2 pseudotyped lentivirus. The results obtained show that peptides designed to block host-pathogen interaction represent a valuable strategy for viral inhibition.

1. Introduction

Viruses represent one of the leading causes of disease and death worldwide. Many viral infections have not only a significant health-related impact on the global community but also on the global economy and the field of antiviral compound discovery is critical to combat viral diseases. Indeed, new antiviral agents are continuously required in the battle against invading viruses. Global pandemic of 2020 was caused by SARS-CoV-2, the causative agent of COVID-19; the COVID-19 pandemic, highlighted the threat posed by viruses and evidenced how strategies for viral infection prevention and control primarily rely on vaccination and antiviral drugs. While vaccination is the preferred intervention and vaccines for COVID-19 are available, this virus continues to spread. Furthermore, immunocompromised people, old people and small children are likely not mounting a robust immune response after vaccination. Thus, novel antiviral therapy should be developed (https://www.state.gov/covid-19-recovery/).

In this context, FDA has approved four antiviral drugs. Veklury (remdesivir) for adults and certain paediatric patients, immune modulators Olumiant (baricitinib) and Actemra (tocilizumab) for certain hospitalized adults and in addition, the oral antiviral pill Paxlovid (nirmatrelvir tablets and ritonavir tablets, co-packaged for oral use) to treat COVID-19 in certain adults (https://www.fda.gov/drugs/emergency-preparedness-drugs/coronavirus-covid-19-drugs). Nonetheless, the development of an even broader class of antiviral agents is crucial.

In SARS-CoV-2 infection, the first step requires the fusion between the viral envelope and host cell membrane, a process mediated by the viral envelope spike (S) glycoprotein (Fig. 1A). All the mechanistic and

* Corresponding authors at: Department of Agricultural Science, University of Naples 'Federico II', Via Università 100, Portici, 80055 Portici, Italy.
E-mail addresses: javier.delamata@uah.es (J. de la Mata), lucia.falcigno@unina.it (L. Falcigno), annarita.falanga@unina.it (A. Falanga).
[1] These authors have contributed equally.

https://doi.org/10.1016/j.ijpharm.2024.124389
Received 21 March 2024; Received in revised form 6 June 2024; Accepted 24 June 2024
Available online 26 June 2024

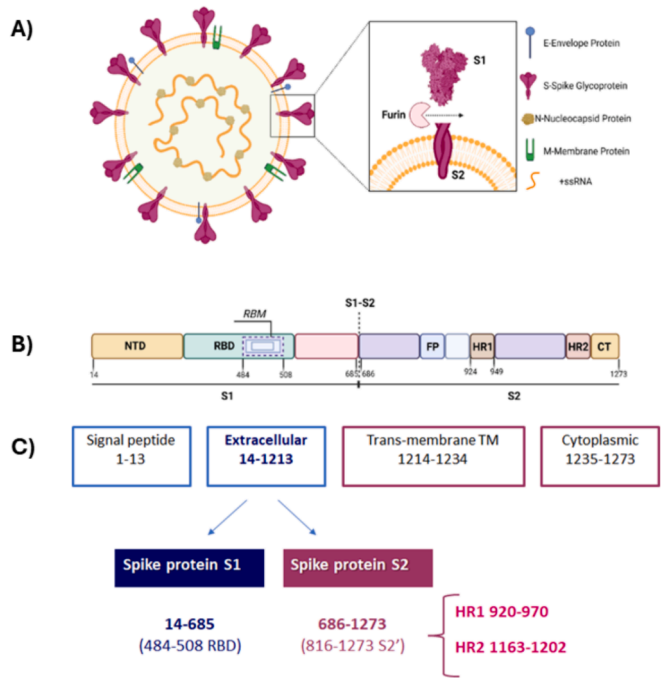

Fig. 1. Coronavirus structure showing the distribution of Spike protein and the zoom of Furin's cut between S1 and S2 subunits (panel A). Primary sequence of Spike protein, highlighting the functional domains for viral infection (panel B). In detail, NTD indicates amino-terminal domain, RBD indicates receptor-binding domain, RBM indicates receptor-binding motif, FP indicates fusion peptide, HR1 and HR2 indicate heptad repeat 1 and 2, respectively and CT indicates carboxy-terminal domain. Schematic representation of Spike glycoprotein S of SARS-CoV-2: 1273 aa Uniprot code P0DTC2 (panel C).

structural aspects of the entry of CoV-2 into human cells are reported in the review by Cody B. Jackson et al. (Jackson et al., 2022). The S protein is a type I fusion protein formed by three monomers, similarly to other enveloped viruses such as human immunodeficiency virus (HIV) (Eckert et al., 1999). Each monomer consists of two subunits, S1 and S2, which further contain several domains (Fig. 1B-C). S2 is anchored to the viral particle through the transmembrane trait (TM), while S1 is outer projected. In brief, cell infection starts with the binding of the receptor-binding domain (RBD) localized onS1 to the angiotensin-converting enzyme 2 (ACE2) present on the host cell. ACE2 was first identified in 2003 as the receptor for SARS- CoV-2 (Shang et al., 2020), and two early crystal structures of the SARS- CoV-2 RBD–ACE2 complex showed how the S protein interacts with its receptor (Lan et al., 2020; Walls et al., 2020).

RBD contains the receptor-binding motif (RBM), a crucial functional segment contributing directly to the attachment to ACE2; its physiochemical properties also affect the binding affinity (Li et al., 2005). The RBM motif consists of amino acids in the S438:Q506 range in SARS-CoV-2, and the x-ray structure of the complex (PDB code 6LZG) (Wang et al., 2020) demonstrates that it approaches the ACE receptor at a distance of 4 Å.

After the virus-cell binding, a complex process of conformational rearrangements leads to the formation of a compact six-helix bundle (6HB) structure, in which each S2 monomer participates with its own heptad repeat units, namely HR1 and HR2. The formation of the 6HB together with a series of other events leads to the close apposition of the TM trait and the fusion peptide (FP), both belonging to the S2 domain, causing the fusion of the viral envelope and the cell membrane. The fusion will allow the transfer of the viral genome into the target cell, transcription, and assembly of new copies of the virus that will be released from the host (Jackson et al., 2022; Shang et al., 2020).

The goal of this paper is the design of new antiviral peptides able to block viral entry filling the important role of preventing initial infection and spread through two different strategies. The first one aims at hampering the initial infection step by blocking the host-pathogen interaction, interfering with the binding between the RBD domain and the ACE2 receptor. For this aim we have selected and synthesized the peptide $RBM_{484\text{-}508}$ located within the highly conserved RBD region (Murdocca et al., 2021), which is expected to antagonize the binding between the virus RBD domain and the ACE receptor. The second strategy is based on the design of a peptide, namely $HR1_{924\text{-}949}$, potentially able to interfere with the formation of the 6HB necessary for the internalization of the virus.

Both the strategies make recourse to peptide sequences that typically may have short half-life and low oral bioavailability due to the rapid degradation by proteases. These problems can be overcome by coupling the peptide of interest to a delivery tool potentially able to slow down the proteases activity and in certain cases also possess their own antiviral activity (Barra et al., 2022; Del Genio et al., 2022a). Dendritic systems are one of the most studied drug delivery tools, being highly branched systems of nanoscopic size and ideally monodispersed. Their specific structure, size, surface charge, functional groups or topologies can significantly influence the interactions with biological systems (Asl et al., 2023; Căta et al., 2023). Among the different types of dendritic systems, carbosilane skeletones provide flexibility and hydrophobicity, essential for interaction with biological membranes (de la Mata et al., 2023). Furthermore, dendritic wedges (dendrons) allow to obtain, in a controlled way, hetero-functionalized systems in which the focal point and the surface groups might have different properties and therefore play a different role or therapeutic action. Here, we used nanosized carriers based on carbosilane dendritic wedges, linked to peptides that inhibit protein–protein interactions. The carbosilane dendrimers are known for their ability to promote solubility in aqueous media thanks to the ionic groups present on their surface and at the same time they also possess antiviral properties by itself (Hernando-Gozalo et al., 2023).

The aim of this work is to analyse the development and therapeutic action of nanoconjugates formed by carbosilane dendritic systems and selected peptides to inhibit the SARS-CoV-2 Spike Protein-Pseudotyped Lentivirus to infect ACE2-expressing HEK293 cells. Our results may come useful for the development of new therapeutic strategies targeting coronavirus infections, and, due to the peculiar structural properties, for potential applications in the field of nanomedicine.

2. Materials and methods

2.1. Materials

All N^{α} –Fmoc-protected conventional amino acids, N,N-diisopropylethylamine (DIEA), piperidine, trifluoroacetic acid (TFA), resins were purchased from Iris Biotech GmbH (Adalbert-Zoellner-Str. 1 D-95615 Marktredwitz). Coupling reagents such as diisopropyl carbodiimide (DIC), (1-[bis(dimethylamino)methyl-ene]-1H-1,2,3-triazolo [4,5-b] pyridinium 3-oxide hexafluoro-phosphate) (HATU), were commercially obtained from GL Biochem Ltd (Shanghai, China).

2.2. Peptide synthesis

We designed two peptide sequences namely: $HR1_{924\text{-}949}$ (1) and $RBM_{484\text{-}508}$ (2). The first one corresponds to the central domain A924-Q949 ($HR1_{924\text{-}949}$) of HR1 located in S2. The other peptide reproduces the segment E484-Y508 of S1 corresponding to the conserved ACE2 binding motif ($RBM_{484\text{-}508}$). A cysteine and Pra (propargylglycine) residues were added at the C-terminus of each peptide for dendrimer conjugation.

The peptides were synthetized with the Fmoc-solid-phase-method (Bellavita et al., 2020). Briefly, all amino acids were protected at their amino terminus with the Fmoc (9-fluorenylmethoxycarbonyl) group and added to the growing chain after the carboxylic acid group activation

(Yousif et al., 2018). Consecutive cycles of amino deprotection in presence of basic solution (20 % piperidine in dimethylformamide, for 10 min, twice) and coupling (four equivalents (equiv) of amino acid and four equiv DIC (Diisopropyl carbodiimide) for the first coupling for 30 min; while four equiv amino acid, four equiv HATU (O-(7-azabenzotriazol-1-yl)-1,1,3,3-tetramethyluroniumhexafluorophosphate) and eight equiv DIPEA (diisopropylethylamine) for the second. The rink amide resin MBHA (4-methyl) benzhydrylamine-resin was used, 0.78 mmol/g. Side chain deprotection and cleavage of the peptides from the resin were achieved using an acid solution of trifluoroacetic acid and scavengers (Falanga et al., 2022). The peptides were precipitated in cold ethylic ether and the crude peptide were analyzed by HPLC–MS using a gradient of acetonitrile (0.1 % TFA) in water (0.1 % TFA) from 20 to 80 % in 20 min. The purified peptides were obtained with a good yield (approximatively 60 %) and their identity were confirmed through Electrospray Ionisation Mass Spectrometry (ESI-MS) (ESI Fig. S1-S4).

2.3. Circular dichroism

Circular dichroism (CD) spectra were recorded at room temperature using a Jasco J-810 spectropolarimeter using the quartz cells (1 and 0.1 cm of path length) from 250 to 195 nm, at room temperature, the spectra are an average of three consecutive scans (Del Genio et al., 2022b). Solution of peptides (100 μM and 8 μM) were collected in buffer and in presence of trifluoroethanol (TFE) at 30 %. Spectra were recorded and corrected for the blank. Mean ellipticities were calculated using the equation Obsd/lc, where Obsd is the ellipticities measured in millidegrees; l is the length of the cell in centimetres; c is the peptide concentration in mol/Liter.

2.4. NMR spectroscopy

RBM_{484}.508-C and $HR1_{924\text{-}949}$-C were NMR analysed in water and TFE/water mixture as well. The samples were prepared by dissolving amounts of peptide in 0.600 mL of H_2O/D_2O (90/10 v:v) or TFE-d3/H_2O (30/70 v:v) to obtain peptide concentrations in the range 0.5 ÷ 0.8 mM (Bellavita et al., 2023). Furthermore, dendrimers functionalized with maleimide or azide moieties and cationic peptide-dendrimer conjugated were analysed in water (H_2O/D_2O 90/10 v:v). NMR spectra were recorded on a Bruker 700 MHz Spectrometer, located at the Department of Pharmacy – University "Federico II" of Naples, and equipped with a z-gradient 5 mm triple-resonance cryoprobe. One-dimensional proton (1D) and two-dimensional homonuclear (2D) NMR spectra were recorded at a temperature of 298 K. The spectra were calibrated relative to TSP (0.00 ppm) as an internal standard. TOCSY (70 ms of mixing time, τm) and NOESY (τm values 100 ÷ 300 ms) spectra were recorded in States phase-sensitive mode, using 4096 and 512 data points in t2 and t1 dimension, respectively. The water resonance was suppressed by use of gradients. NMR spectra were analysed by CARA program. (https://cara.nmr.ch/doku.php/home) Proton assignments (ESI Tables S1-S5) were obtained by classical methodology (Wüthrich, 1986).

2.5. Structure determination

The structures adopted by $RBM_{484\text{-}508}$-C and $HR1_{924\text{-}949}$-C in the two different solvent media were obtained starting from integration of NOESY spectra acquired with 300 ms as τm. The NOE cross-peaks were integrated with CARA software and converted into distance upper limits, via CALIBA (Güntert et al., 1991), adopting the geminal protons of selected residues fixed at 2.2 Å as distance reference. Structure calculations were performed by CYANA 100 randomized conformers were generated and submitted to simulated annealing schedule with 20,000 torsion angle dynamics steps per conformer. The calculus converged at conformers showing a fairly agreement with experimental constraints with no distance violations. The CYANA structures with the best agreement with experimental data, i.e., those with lowest target function (TF) values (statistical analyses of the structures are reported in ESI Table S4,), were chosen to represent the peptide molecular structures in solution. MolMol (Koradi et al., 1996) software was used to analyse the structures and Chimera (Pettersen et al., 2004) to clustering them by similarity. Chosen 3D models were visualized by PyMOL software (DeLano, 2002).

2.6. Synthesis of carbosilane dendrons and nanoconjugates carbosilane dendron–peptide

The dendritic wedges of second generation with maleimide, $MalG_2(S(CH_2)_2NMe_2HCl)_4$ (5) or azide moieties at focal point $N_3(S(CH_2)_3SO_3Na)_4$ (8) selected for this work are described in the literature (Fernandez et al., 2019). The molecular structures of dendrons are shown in Fig. 7. Solvents were dried and freshly collected from a purification system of MBraun-SPS.

2.6.1. Cationic nanoconjugates

To obtain the compounds $HR1_{924\text{-}949}$-C-$G_2(S(CH_2)_2NMe_2HCl)_4$ (3) and $RBM_{484\text{-}508}$C-$G_2(S(CH_2)_2NMe_2HCl)_4$ (4), thiol-maleimide addition coupling reaction were employed (Ravasco et al., 2019) for nanoconjugate 3, a water solution, previously deoxygenated with argon, of dendron $MalG_2$ $(S(CH_2)_2NMe_2HCl)_4$ (1.14 mg, $1.098*10^{-6}$ mol) was added drop by drop over the peptide $HR1_{924\text{-}949}$. cdissolved in 2 mL of water (3.3 mg,$1.098*10^{-6}$mol). The mixture was stirred at room temperature for 48 h. After that, solvent was evaporated and the conjugate HR1-$C_{924\text{-}949}$-C-$G_2(S(CH_2)_2NMe_2HCl)_4$ (3) was obtained as a white-yellowish solid (4.7 mg). The same protocol was carried out for nanoconjugate $RBM_{484\text{-}508}$- C-$G_2(S(CH_2)_2NMe_2HCl)_4$ (4) starting to 1.41 mg ($1.36*10^{-6}$ mol) of $MalG_2$ $(S(CH_2)_2NMe_2HCl)_4$ and 3.8 mg ($1,36*10^{-6}$mol) of the peptide $RBM_{484\text{-}508}$-C. The nanoconjugate $RBM_{484\text{-}508}$-C $-G_2(S(CH_2)_2NMe_2HCl)_4$ (4), was obtained as a white-yellowish solid (5.2 mg)

2.6.2. Anionic nanoconjugates

To obtain the compounds $HR1_{924\text{-}949}$-PRA cK-$G_2(S(CH_2)_3SO_3Na)_4$ (6) and $RBM_{484\text{-}508}$-PRA cK-$G_2(S(CH_2)_3SO_3Na)_4$ (7) the azide-alkyne Huisgen cycloaddition ("Click chemistry") strategy were used (Breugst and Reissig, 2020) for nanoconjugate $HR1_{924\text{-}949}$-PRA-cK-$G_2(S(CH_2)_3SO_3Na)_4$ (6) a solution of dendric wedge $N_3(S(CH_2)_3SO_3Na)_4$ 1,4 mg ($1,18x10^{-6}$ mol) and peptide $HR1_{924\text{-}949}$-PRA (3.3 mg; $1.18*10^{-6}$ mol) in water, were deoxygenated with argon, was stirred at room temperature for 48 h in presence of Et_3N (1 drop) and CuI as catalyst (5 % mol/ by the propyl moieties). After that, the compound was dialyzed using a 100–500 da membrane in distilled water under stirring for 3 days to remove the CuI. Finally, solvent was evaporated and the conjugate $HR1_{924\text{-}949}$-PRA .cK-$G_2(S(CH_2)_3SO_3Na)_4$ (6), was obtained as a white solid (4,68 mg) and characterized

The same protocol was carried out for nanoconjugate $RBM_{484\text{-}508}$-PRA $-N_3(S(CH_2)_3SO_3Na)_4$ (**7**) starting to compound $N_3G_2(S(CH_2)_3SO_3Na)_4$ (1.27 mg ($1.07*10^{-6}$ mol), peptide $RBM_{484\text{-}508}$-PRA (3.2 mg, $1.07*10^{-6}$ mol), Et_3N (1 drop) and CuI as catalyst (5 % mol/ by the propyl moieties) to obtain the nanoconjugate $RBM_{484\text{-}508}$-PRA $-N_3(S(CH_2)_3SO_3Na)_4$ (**7**) as a white solid (4.46 mg).

2.7. Cytotoxicity

Cell viability was measured using the MTT assay. Briefly, cells were grown in 96-well plates and treated with for 48 h with different concentration of the dendrimers and peptide-dendrimer conjugates. The untreated cells were used as controls. The culture medium was then removed and replaced with fresh medium (without FBS) containing 0.5 μg ml^{-1} tetrazolium salt (MTT, 5 mg/ml, Sigma Alrich, M5665). After 48 h of treatment the cells were incubated for 3 h at 37 °C in 5 % CO_2, protected from light, and the precipitated formazan was solubilized with DMSO (Sigma Aldrich, D8418). The absorbance was measured at 540

nm using a microplate reader. Four replicates were measured for each sample.

2.8. Lentiviral production and cells transduction

To test the ability of synthetized peptides to prevent the SARS-CoV-2 infection we generated a SARS-CoV-2 Spike Protein-Pseudotyped Lentivirus to infect ACE2-expressing HEK293 Cells. Lentiviral particles pseudotyped with the SARS-CoV-2B.1.1.529 (Omicron) variant were packaged in HEK293T cells using third-generation packaging plasmids provided by Cellecta plus (CA), a homemade genome lentiviral plasmid containing a luciferase expression cassette, according to the manufacturing protocol (Passariello et al., 2023). The Cells (4×10^6) were plated in 10-cm plates with 10 ml of media for 24 h prior to transfection and then the Packaging Plasmid Mix (0.5 μg/μl) and plasmids carrying a reporter expressing luciferase were co-trasfected in cells by lipofectamine 2000 transfection reagent (ThermoFisher, Italy). 5 h post-transfection, medium containing complexes was replaced with 10 ml of fresh D-MEM medium and the virus-containing medium was collected after 24-, 48- and 72-h from each plate and centrifuged at 1200 rpm to remove debris and floating packaging cells. Then the titer of harvested SARS-CoV-2 Spike Protein-Pseudotyped Lentivirus particles was quantified by Droplet Digital PCR.

2.9. RNA extraction and quantization of viral particles by Droplet digital PCR (ddPCR)

To quantify the pseudovirus titer, 100 μl of supernatant containing lentiviral particles was mixed to an equal volume of Quick extract RNA solution (Lucigen) to extract RNA, and incubated at 95 °C for 5 min. Then 15ul of extracted RNA was used for retrotranscription reaction to generate cDNA, consequently assembled in a Digital Droplet PCR reaction with EvaGreen Mastermix (Biorad, Italy), using the following primers for luciferase gene detection: Forward AAGAGGCGAACTGTGTGTGAGA and reverse ATGTAGCCATCCATCCTTGTCA. After the PCR step of previously generated droplets, the positive droplets were detected using a QX200 Droplet Reader (BioRad, Feldkirchen, Germany) and the number of viral particles was calculated using QuantaSoft Software version 1.7.4. Droplet Digital PCR thermal cycling conditions used for the assay are reported in Table 1.

2.10. Anti-viral activity evaluation

HEK293–hACE2 cells seeded in 96 multiwell plate, at 70 % of confluence were infected for 48 hrs with pseudovirus expressing the luciferase as reporter gene ($1x10^6$ particles) together with one of the eight different compounds (see Fig. 9): $HR1_{924\text{-}949}$ (**1**), $RBM_{484\text{-}508}$ (**2**), dendrons $MalG_2(S(CH_2)_2NMe_2HCl)_4$ (**5**) and $N_3(S(CH_2)_3SO_3Na)_4$ (**8**); nanoconjugates HR1-$C_{924\text{-}949}$-C-$G_2(S(CH_2)_2NMe_2HCl)_4$ (**3**), $RBM_{484\text{-}508}$-C–$G_2(S(CH_2)_2NMe_2HCl)_4$ (**4**), $HR1_{924\text{-}949}$-PRA cK-$G_2(S(CH_2)_3SO_3Na)_4$ (**6**) and $RBM_{484\text{-}508}$-PRA − cK-$G_2(S(CH_2)_3SO_3Na)_4$ (**7**). The eight compounds were tested in three different assay combinations: A (neutralization assay), B (preventive treatment) and C (therapeutic treatment) at 25 μM of each compound.

Table 1
Droplet digital reaction Program.

Droplet digital reaction Program				
Step	**Temperature**	**Time**	**Ramp Rate**	**cycles**
Initial denaturation	95°C	10 min	2,5°C/sec	1
Denaturation	95°C	30 s		40
Annealing	55°C	30 s		
Extension	72°C	15 s		
Signal stabilization	98°C	10′		1
Hold (optional)	12°C	infinite		1

For all experimental settings, cells were lysed after 48 h post-infection with 40 μl of Passive lysis buffer (PLB) (Promega, Italy) and stored at −80 °C overnight. Then, the plate was shifted at RT for 20 min and then at −80 °C for further 20 min. To analyze luciferase activity, 10 μL of lysate were loaded into a black flat bottom Costar 96-well plate and 35 μl of Luciferase Assay Reagent II (LAR II) were dispensed to each well to generate a luminescent signal. The expression of a luciferase reporter was quantified as the luminescence produced above background level by PHERAStar FSX reader, BMG LABTECH, Germany. After bioluminescence analyses, the percentage of infectivity was measured. Non-infected cells or cells treated with only pseudoviruses were used as negative and positive control respectively. All the data are reported as means ± SD. Statistical significance was defined by unpaired two-tailed Student's t-tests and represented as follows: * $p < 0.05$, ** $p < 0.001$.

3. Results and discussions

3.1. Peptide design

We designed two peptide sequences belonging to Spike protein: i) the first one involved in ACE2 recognition and corresponding to E484-Y508 belonging to RBM (438–506 residues) of S1, namely $RBM_{484\text{-}508}$ (Sun et al., 2020). ii) the second one namely $HR1_{924\text{-}949}$, corresponding to the fragment A924-Q949 of HR1, which is involved in the interaction with HR2 in the 6HB assembly. The choice of these sequences was based on the knowledge of the molecular structures and dynamics dictating the mechanism of the virus entry into the host cell. PDB data bank contains numerous structures of protein S fragments, integer monomer, trimers in different states (inactive, active), and complexes that describe pre-steps of the fusion process. Based on these structures, an infection mechanism like that typical of class I fusion proteins can be traced (Jackson et al., 2022). Each S monomer in the trimer is formed by two non-covalently linked subunits (protein S is cleaved into the two subunits inside the host). The S trimer is spatially oriented with three S1 domains outward-exposed and the backward-oriented S2 domains that anchor the whole complex to the virus through TM segments. By dynamic motions, S trimer may expose the RBD from one or more of its monomers (Zhang et al., 2020). The binding of RBD by ACE2 cell receptor produces the virus-cell anchorage. This event causes exposition of the 630 loop and FP-PR (Fusion Peptide Proximal Region) site. The 630 loop dislocation destabilizes the un-covalently bound S1/S2 complex with leaving of S1 from S2. FP-PR site also dislocates, causing the exposition of the S2 site whose cleavage makes the FP free. HR1 rearrangement pushes the FPs into the cell membrane (Fan et al., 2020) while, the three HR2 segments fold back forming 6HB with HR1. This bundle drags TM close to FP making possible the fusion.

Our aim was to select the shortest sequences able to block the protein- protein interactions that take place during virus attachment, with two different strategies. $RBM_{484\text{-}508}$ was designed to compete (antagonize) with viral RBD for the ACE2 binding, while HR1924-949 to prevent the assembly of the coiled coil super-structure 6HB and thus the process of virus-host membrane fusion (Lan et al., 2020).

3.2. NMR characterization of $RBM_{484\text{-}508}$-C peptide

The structure of $RBM_{484\text{-}508}$-C was analysed via NMR in water and in TFE/water mixture. In water the peptide is poorly organized. The diagnosis comes from the comparison between the chemical shift data (Table S1, ESI Fig. S5) and the pattern of NOE effects (ESI Fig. S6). The chemical shift deviations from random coil values (Wishart et al., 1992) of αCH protons, ΔδαCH, of $RBM_{484\text{-}508}$ in water are positive and occasionally close to zero (ESI Fig. S5, blue bars), thus indicating a mixture of disordered structures including short traits in extended conformation localized where the deviations exceed + 0.1 ppm. No structure changes are observed moving the peptide from plain water to alcoholic/H_2O mixture, as indicated by chemical shift (Table S2 and ESI Fig. S5, fuchsia

bars) and NOE data (ESI Fig. S6). The molecular models were computed by CYANA program (Güntert, 2004) using NOE derived distances (ESI Fig. S6) as upper limit (upl) of interproton distances for $RBM_{484\text{-}508}$ in water and TFE/H_2O. The best CYANA structures in terms of agreement with experimental data, i.e., with lowest target function (TF) values (ESI Table S5), were clustered by similarity and the first clusters were chosen as representative of the conformational space covered by the peptide in each environment (Fig. 2).

Overall, the NMR analysis reveals a flexible and disordered structure for $RBM_{484\text{-}508}$ peptide, even in the presence of "structuring" TFE. This result well agrees with the flexible and poorly ordered structure of the RBM in the native Spike glycoprotein. In fact, RBM is a loop and for that hasthose conformational adaptation properties necessary to bind the ACE2 receptor (Fig. 3).

3.3. NMR characterization of $HR1_{924\text{-}949}$ peptide

Differently from $RBM_{484\text{-}508}$, the NMR structure of $HR1_{924\text{-}949}$ depends on the solvent medium in which it is dissolved. In water the peptide is poorly organized even though not completely random. Indeed, the chemical shift deviations from random coil values of αCH protons (Wishart et al., 1992), ΔδαCH, of $HR1_{924\text{-}949}$ in water are positive and occasionally close to zero (ESI Fig. S7, green bars, Table S3), so indicating of the occurrence of disordered structures, whilst the NOE pattern (ESI Fig. S8a) shows the presence of medium range NOE effects which testifies the $HR1_{924\text{-}949}$ propensity to adopt a helical structure even in plain water. Globally, chemical shift and NOE data in water indicate that $HR1_{924\text{-}949}$ interconverts among different structural elements including extended and helix traits.

In a less hydrophilic environment as TFE/H_2O, the propensity of $HR1_{924\text{-}949}$ to adopt a helical structure is confirmed by both the chemical shift deviations, which are mainly negative (ESI Fig. S7, violet bars and Table S4), and by the number and intensity of the NOE effects (ESI Fig. S8b). The molecular models were computed by CYANA program using NOE derived distances (ESI Fig. S8) as upper limit (upl) of interproton distances for $HR1_{924\text{-}949}$ in water and TFE/H_2O. The best CYANA structures in terms of agreement with experimental data, i.e., with lowest target function (TF) values, were clustered by similarity and the first clusters were chosen as representative of the conformational space covered by the peptide in each environment (Fig. 4). Globally, the NMR analysis indicates a helical structure of $HR1_{924\text{-}949}$ in the alcoholic medium mimicking the biological environment. Once more, this result fairly agrees with the ordered helix structure of the HR1 moiety in the native Spike glycoprotein.

111898063731600$HR1_{924\text{-}949}$ corresponds to the HR1 region in hydrophobic contact with HR2 in the super-coiled structure. The superposition of the representative NMR/CYANA structure of $HR1_{924\text{-}949}$ in TFE 30 % (purple) to the sequence 924–949 of 6m1v X-ray structure, gives RMSD values of 5.41 Å and 2.36 Å, respectively (Fig. 5). A comparison with the other X-ray structures gives back similar RMSD values.

It's worth noticing that the $HR1_{924\text{-}949}$ peptide well reproduces the pattern of hydrophobic as well as hydrophilic interactions of the 6HB in the X-ray structures (Fig. 5).

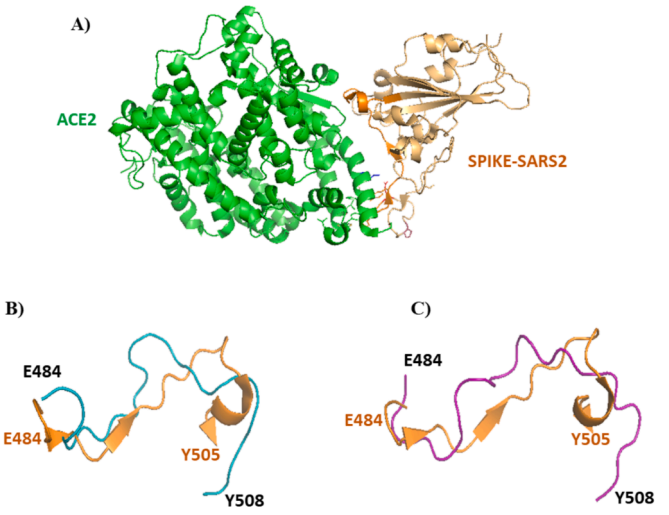

Fig. 3. X-Ray structure of SPIKE- SARS-CoV-2 (orange) in complex with human receptor ACE2 (green 6LZG) from Wang et al. Cell 2020 (Wang et al., 2020) (panel A) Superposition of the representative NMR structures of $RBM_{484\text{-}508}$ in water (cyan) (panel B) and in TFE 30% (purple) (panel C) with the native RBM sequence E_{484}-Y_{508} (orange) of 6LZG X-ray complex. (For interpretation of the references to colour in this figure legend, the reader is referred to the web version of this article.)

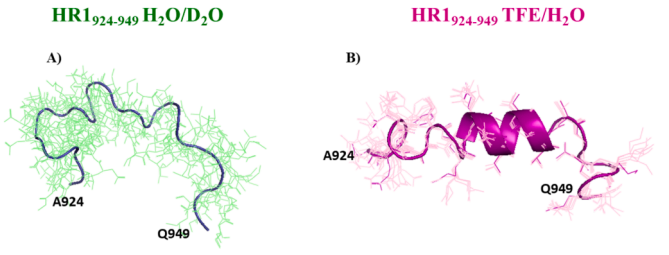

Fig. 4. NMR structures of HR1924-949 A) in H2O/D2O 90/10 and B) in TFE/H2O 30/70, clustered by CHIMERA and visualized by PYMOL. For each cluster, all structures are shown as lines and the representative structure as cartoon.

3.4. Circular dichroism

The structure of $RBM_{484\text{-}508}$ and $HR1_{924\text{-}949}$ were also analysed via circular dichroism in phosphate buffer and in TFE/water mixture. In buffer, the peptide $RBM_{484\text{-}508}$ is unfolded (Fig. 6, panel A) while when decreasing the environmental polarity using aqueous mixtures of TFE (Fig. 6, panel C) the peptide shows a slight tendence to adopt an alpha

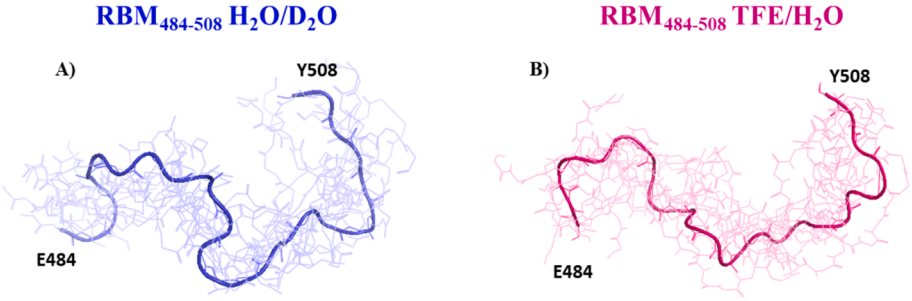

Fig. 2. NMR structures of $RBM_{484\text{-}508}$-C in H_2O/D_2O 90/10 (panel A) and in TFE/H_2O 30/70 (panel B), clustered by CHIMERA and visualized by PYMOL. For each cluster, all structures are shown as lines and the representative structure as cartoon.

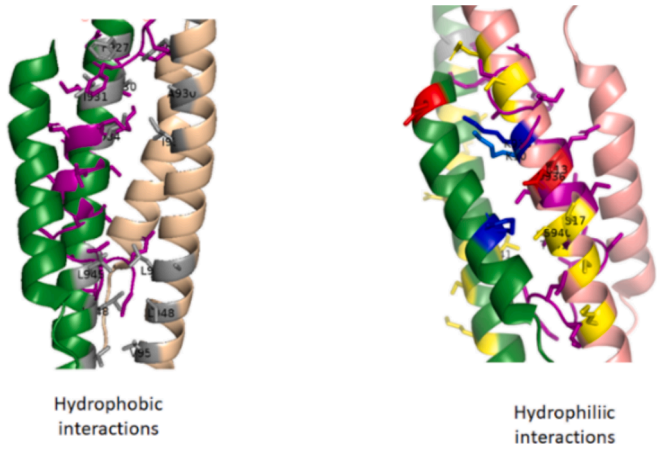

Fig. 5. The superposition of the representative NMR/CYANA structure of $HR1_{924-949}$ in TFE 30% (purple) to the sequence 924–949 of 6m1v X-ray structure.

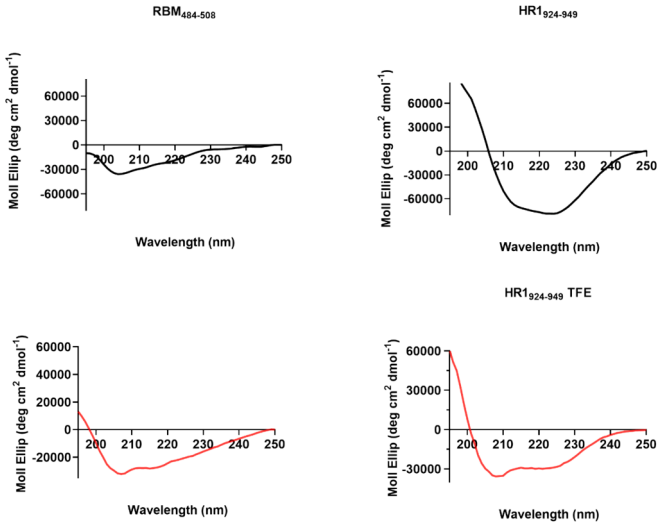

Fig. 6. Secondary structure of $RBM_{484-508}$ in water (panel A) and in a solution of TFE and water (30/70 v/v) (panel C); secondary structure of $HR1_{924-929}$ in water (panel B) and in a solution of TFE and water (30/70 v/v) (panel D).

helix conformation. Furthermore, the peptide $HR1_{924-949}$ shows an aggregated helical structure in water (Fig. 6, panel B). In the presence of TFE the CD profile shows two minima at 208 and 222 nm with the one at 222 nm more pronounced typical of aggregated α-helical structure.. Indeed, the presence of TFE reduces the hydrophobic interactions among helical domains and favours helical monomeric structures, as evidenced by the more pronounced minimum at 208 nm. (Fig. 6, panel D) (Maroun et al., 1999).

3.5. Peptide- dendrimers characterization

We analysed the formation of peptide-dendrimer nanoconjugates where the two moieties were coupled by covalent bonds. The selected peptides, $HR1_{924-949}$ and $RBM_{484-508}$, were derivatized with a cysteine or propargyl group (Table 2). To allow the formation of the conjugates by thiol-maleimide and azide-alkyne Huisgen cycloaddition to dendrons with maleimide or azide at the focal point, respectively (Fig. 7). The successful formation of the thiol-maleimide conjugates was verified by NMR measurements. The comparison of proton NMR spectra of the positively charged dendrimer free (5) and loaded with peptide $RBM_{484-508}$-C is shown in ESI Fig. S10. The disappearance of maleimide alkene

Table 2
Sequences of synthetized peptides $RBM_{484-508}$ and $HR1_{924-949}$modified to bear a C-terminal Cys (C) or propargylglycine (PRA).

Compound	Sequence
$rbm_{484-508}$-c	Ac-E^{484}GFNSYFPLQSYGFQPTNGVGYQPY^{508} −C-$CONH_2$
$rbm_{484-508}$-pra	Ac-EGFNSYFPLQSYGFQPTNGVGYQPY-Pra-$CONH_2$
$hr1_{924-949}$-c	Ac-ANQFNSAIGKIQDSLSSTASALGKLQ-C-$CONH_2$
$hr1_{924-949}$-pra	Ac-ANQFNSAIGKIQDSLSSTASALGKLQ-Pra-$CONH_2$

protons at 6.66 ppm and the presence of protons of succinimide ring at 3.7 ppm indicate that the peptide-dendrimer conjugation was successfully achieved.

However, it is worth noting that the NMR analyses cannot exclude the further occurrence of non-covalent interactions between the charges present on the peptide and the ionic groups on the surface of the dendritic wedge. The conjugates appear very stable over the time as verified by NMR spectra acquired over a period of months (Fig. ESI S10).

3.6. Anti-Viral activity evaluation

The antiviral activity of free peptides, free dendrimers and peptide-dendrimer was evaluated through the use of SARS-CoV-2 pseudotyped lentivirus. As shown in Fig. 8, after the production of the virus,we infected ACE2-expressing HEK293 cells for 48 h with pseudovirus expressing the luciferase together with or without the peptides/dendrimers/peptide-dendrimers.

We tested a series of eight compounds that include the two free peptides $HR1_{924-949}$ (**1**) and $RBM_{484-508}$ (**2**), the two peptides bound to each dendrimer: HR1-$_{924-949}$-C-$G_2(S(CH_2)_2NMe_2HCl)_4$ (**3**), RBM-$_{484-508}$-C-$G_2(S(CH_2)_2NMe_2HCl)_4$ (**4**), $HR1_{924-949}$-PRA −cK-$G_2(S(CH_2)_3SO_3Na)_4$ (**6**) and $RBM_{484-508}$-PRA − cK-$G_2(S(CH_2)_3SO_3Na)_4$ (**7**), and the dendrimers alone $MalG_2(S(CH_2)_2NMe_2HCl)_4$ (**5**) and $N_3(S(CH_2)_3SO3Na)_4$ (**8**).

To determine the optimal compound concentration for the experiments, we conducted preliminary experiments using three different concentrations: 12.5 μM, 25 μM, and 50 μM. It was observed that many compounds exhibited toxicity at the 50 μM concentration, whereas at the lower concentration of 12.5 μM, several compounds showed inactivity (Data not shown). Consequently, the intermediate concentration of 25 μM was selected for subsequent experiments.

All compounds were tested in three different experimental setups: **A** as neutralization assay, in which virus was incubated with the compounds for 30 min before to be used to infect the cells; **B** as preventive treatment, in which cells were incubated with the compounds for 30 min before to be infected by the virus; **C** as therapeutic treatment, in which cells were infected by the virus and after 30 min treated with the compounds. We obtained different antiviral activity depending on both compound and setup used. As concerns the neutralization assay (setup A), the best antiviral activity is observed for free peptide $RBM_{484-508}$ (about 50 %) and for $RBM_{484-508}$ bound to the positively charged MalG2 (S(CH2)2NMe2HCl)4 dendrimer (about 70 %), compounds 2 and 4 in Fig. 9. This result can be explained by considering that when the pool virus + compound encounters the cells, the RBM site of viral Spike protein and the $RBM_{484-508}$ peptide compete for the binding to the ACE2 cell receptor. Moreover, the better activity of $RBM_{484-508}$ peptide bound to the positively charged dendrimer MalG2(S(CH2)2NMe2HCl)4 is due to a better exposure of the compound to the cell surface. Furthermore, it is known that positively charged particles interact more with cell membranes compared to neutral or negatively charged ones (Forest and Pourchez, 2017). Regarding the $HR1_{924-929}$ peptide, we found it to be ineffective in both the free and conjugated forms. We believe that in the isolated virus the HR sequence is not yet exposed on the surface of the virus and therefore, when the virus is pre-treated with $HR1_{924-929}$ and its conjugates, $HR1_{924-929}$ peptide cannot play a functional role.

Regarding cell preventive treatment with our compounds (setup B),

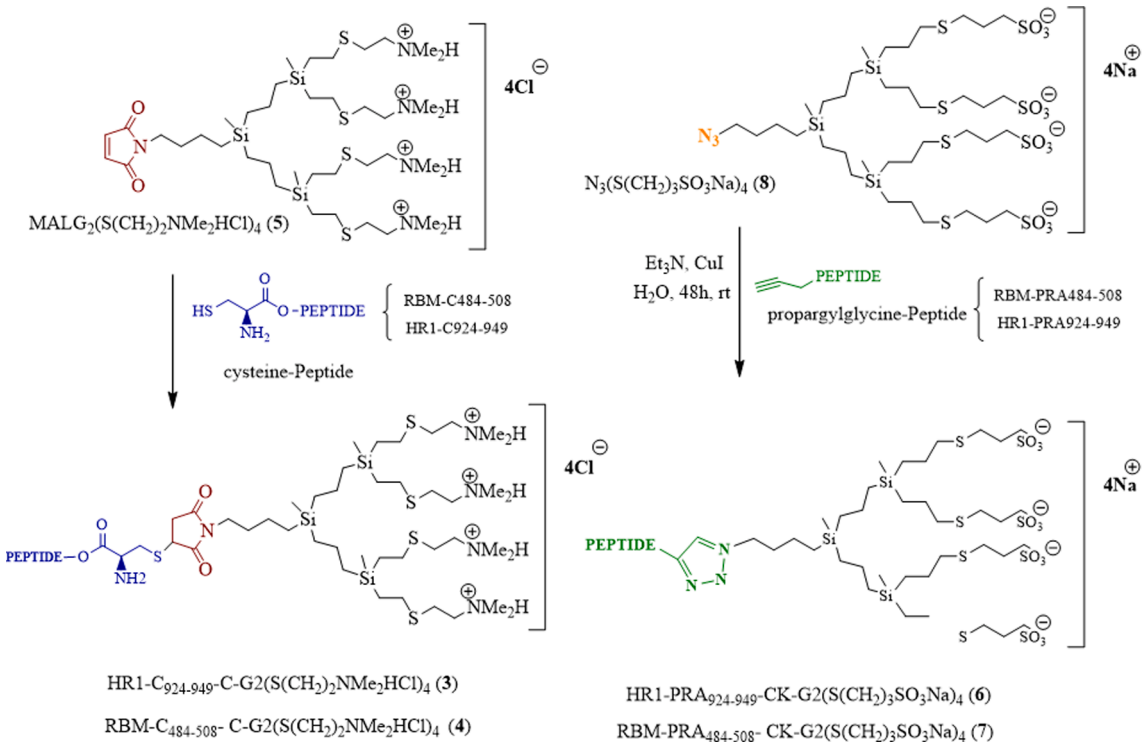

Fig. 7. Schematic representations of peptide-dendrimer nanoconjugates. Left: negatively charged dendrimer functionalized with azide (top) and covalently linked to peptides $RBM_{484\text{-}508}$ and $HR1_{924\text{-}949}$ functionalized with proargylglycine group (bottom). Right: positively charged dendrimer functionalized with maleimide (top) and covalently linked to peptides $RBM_{484\text{-}508}$ and $HR1_{924\text{-}949}$ functionalized with cysteine (bottom).

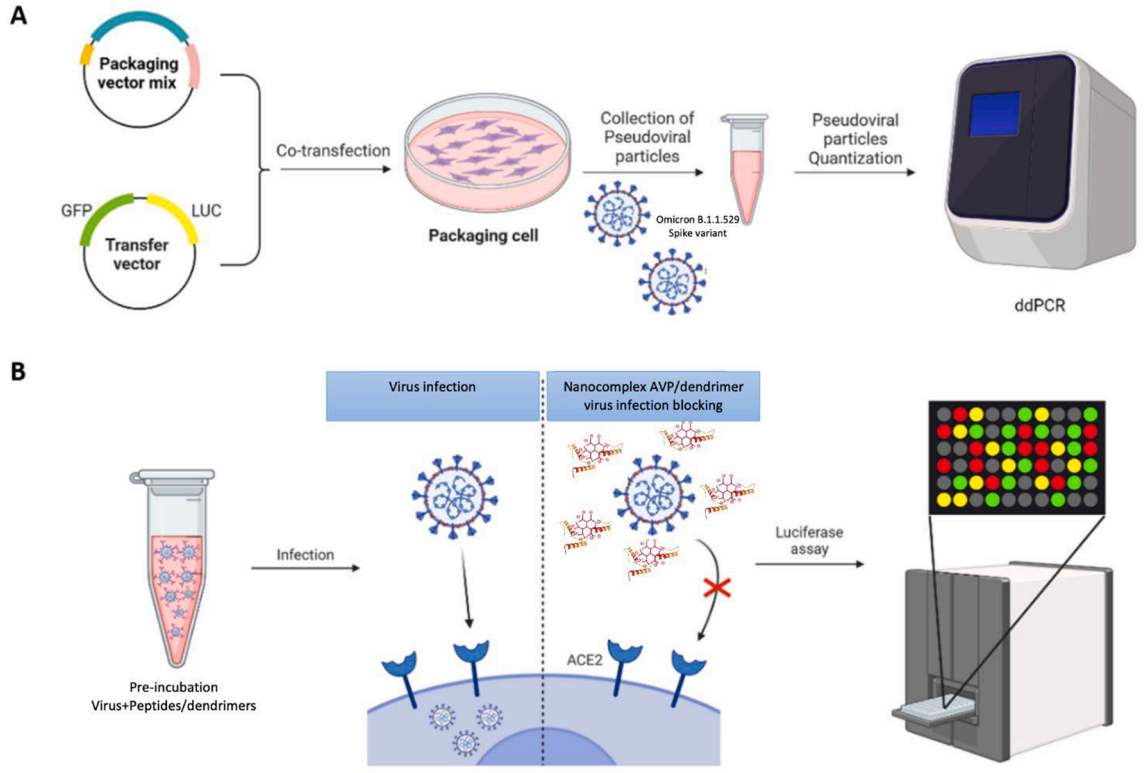

Fig. 8. Schematic representation of Pseudoviral particles preparation process and antiviral activity assay. (A) Pseudoviruses expressing Omicron Spike protein were produced in packaging cells co-trasfected with the reporter vector expressing luciferase and green fluorescent protein and the packaging vector mix. Cell supernatants containing pseudoviral particles were collected at different times and the virus titer quantified by ddPCR. (B) The antiviral activity of peptides/dendrimers/peptide-dendrimers was tested by luciferase activity evaluation in infected cells. (For interpretation of the references to colour in this figure legend, the reader is referred to the web version of this article.)

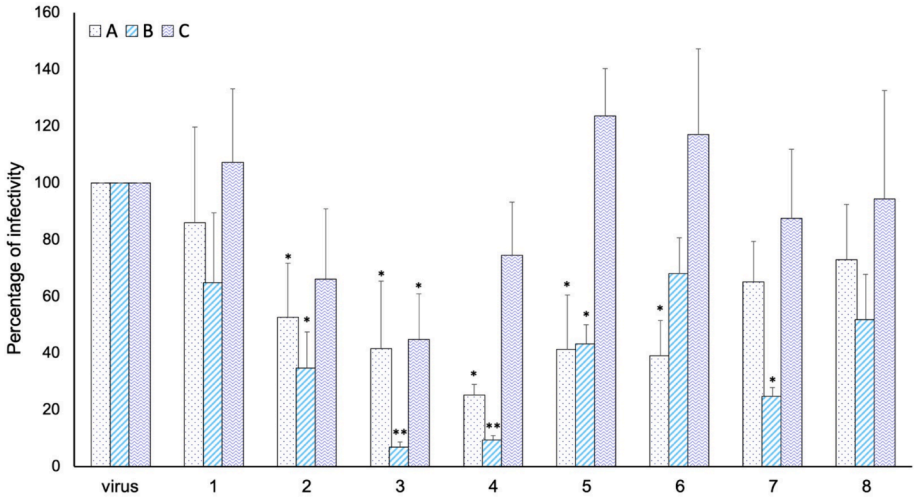

Fig. 9. Antiviral activity of peptide-dendrimers on Omicron BA.1-derived pseudoviruses in cell cultures. Pseudoviruses expressing Omicron Spike variant protein were pre-incubated with 25 μM of peptides or dendrimers o complexes of both, for 1 h at 37 °C. (1 = $HR1_{924\text{-}949}$, 2 = $RBM_{484\text{-}508}$, 3 = $HR1_{924\text{-}949}$-C-$G_2(S(CH_2)_2NMe_2HCl)_4$, 4 = RBM484-508-C −$G_2(S(CH_2)_2NMe_2HCl)_4$, 5 = $MalG_2(S(CH_2)_2NMe_2HCl)_4$, 6 = $HR1_{924\text{-}949}$-PRA −cK-$G_2(S(CH_2)_3SO_3Na)_4$, 7 = $RBM_{484\text{-}508}$-PRA −cK-$G_2(S(CH_2)3SO_3Na)_4$, 8 = $N_3(S(CH_2)_3SO_3Na)_4$). Then, HEK293-ACE2 cells were infected with the mixtures for 48 h and the levels of infectivity expressed as percentage of luminescence with respect to untreated infected cells used as a positive control. Error bars shown are means ± SD and were obtained by at least three independent experiments. p-value: * $p < 0.05$, ** $p < 0.001$ by unpaired two-tailed Student's t-tests.

we found that the results of antiviral activities improve in the order:

$HR1_{924\text{-}949}$-C-$G_2(S(CH_2)_2NMe_2HCl)_4$ (**3**), $RBM_{484\text{-}508}$C-$G_2(S(CH_2)_2NMe_2HCl)_4$ (**4**), $RBM_{484\text{-}508}$-PRA- cK-$G_2(S(CH_2)_3SO_3Na)_4$ (**7**), $RBM_{484\text{-}508}$ (**2**), (Fig. 9). We note here that both $RBM_{484\text{-}508}$ alone and bound to the negatively charged dendrimer $N_3(S(CH_2)_3SO_3Na)_4$ show a comparable anti-viral activity, while when bound to the positively charged dendrimer $MalG_2(S(CH_2)_2NMe_2HCl)_4$ shows a very high antiviral activity reducing infectivity by 90 %. Indeed, $RBM_{484\text{-}508}$ was designed to bind the ACE2 cell receptor and seems to do it very well when it is bound to the positively charged dendrimer $MalG_2(S(CH_2)_2NMe_2HCl)_4$ (**4**). Therefore, when the virus is added to the pre-treated cells with our compounds (setup B), it finds few ACE2 cell receptors available for binding to, and consequently, few chances to be infective. The same significant antiviral activity is shown by $HR1_{924\text{-}929}$ bound to the positively charged dendrimer $MalG_2(S(CH_2)_2NMe_2HCl)_4$. HR1 sequence, as already said, was designed to disturb the assembling of 6HB. The formation of 6HB is a late event in the fusion mechanism. We believe that the peptide bound to the dendrimer can dock on the cell surface. Therefore, when the virus is added, the presence of $HR1_{924\text{-}929}$ may disturb proper 6HB formation and the fusion and infection. Another possible interpretation of the result is that $HR1_{924\text{-}929}$ internalized in the cell thanks to the dendrimer can interfere in the correct folding of the Spike protein. It is possible that one or the other of the processes occurs or that both are active at the same time.

Finally, in the protocol C, the activities of the different compounds are evaluated on cells pre-infected by the virus (therapeutic treatment). We find that just $HR1_{924\text{-}949}$ when linked to the positively charged $MalG_2(S(CH_2)_2NMe_2HCl)_4$ shows some antiviral activity. One possible interpretation of this result is that $HR1_{924\text{-}949}$ acts only on that percentage of cells not yet infected by the virus and that are still in course of fusion. At this stage $HR1_{924\text{-}949}$ influences the correct assembly of 6HB. Moreover, as said above, $HR1_{924\text{-}949}$ bound to the dendrimer, may internalize in the cells already infected, and interfere with Spike protein correct folding.

4. Discussion and conclusion

Here we have designed and synthetized a series of peptides, dendrimers and peptide-dendrimers as tools to inhibit SARS-CoV-2 viral infections. As concerns the peptide moieties, we choose two sequences: $RBM_{484\text{-}508}$ and $HR1_{924\text{-}949}$, potentially able to interfere with the binding to human ACE2 receptor and with the virus cell membrane fusion, respectively. Dendrimers themselves present antifungal, antibacterial and antiviral activities (Falanga et al., 2021; Sherje et al., 2018). Moreover, their structural versatility and the easy to control their chemical-physical features give them special properties and make them ideal carriers for many active molecules. Indeed, to improve peptides stability and antiviral activities, we used dendrimers as peptide carriers. Furthermore, negative carbosilane dendrimers have been shown to be potent antivirals against HIV or syncytial virus due to their ability to block specific proteins of viral capsids used to anchor to host cells or receptors in the host cells. [36] For this reason, the presence of negative charges in dendritic wedge $N_3(S(CH_2)_3SO_3Na)_4$ (**8**) could establish possible collaborative or synergistic effects derived from the antiviral activity that both systems, dendron and peptide, present separately.

Free peptides ($RBM_{484\text{-}508}$ and $HR1_{924\text{-}949}$), free dendrimers (negatively and positively charged), and the four combinations of peptide-dendrimers (Fig. 7) were structurally characterized and tested for their anti-viral activities.

CD and NMR analyses of $RBM_{484\text{-}508}$ and $HR1_{924\text{-}949}$ indicate that they well reproduce the structure they adopt in the native Spike glycoprotein. Indeed, $RBM_{484\text{-}508}$ is unstructured, as expected for a fragment belonging to a flexible loop of Spike glycoprotein deputed to recognize ACE2 cell receptor. On the other hand, $HR1_{924\text{-}949}$, presents an ordered helical structure, the same that it adopts in the Spike glycoprotein. These peptides, both alone or conjugated to positively and negatively charged dendrimers, were tested for their antiviral activities. The antiviral activities were evaluated, as described above, through three different experimental setups: A) virus pre-incubated with each compound before to cell infection (neutralization assay); B) cells pre-incubated with each compound before virus infection (preventive treatment); C) cells infected by virus followed by compound addition (therapeutic treatment). overall, the best antiviral activities were found when cells were pre-treated with our compounds before virus infection (setup B). As concerns the free peptides, the best antiviral activity is observed for $RBM_{484\text{-}508}$ in preventive treatment B, i.e. when it is pre-incubated with cells before virus addition. This result can be explained by considering that $RBM_{484\text{-}508}$ binds to ACE2 cell receptor, depriving the Spike protein of availability of all contact sites. By considering the same experimental preventive setup, $RBM_{484\text{-}508}$ antiviral performance is even better when

it is bound to dendrimers, and in particular when bound to the positively charged dendrimer. These findings confirm the role of dendrimers in favoring the close approach of the peptide to the cell membrane and also prove that positively charged particles better interact with cell membranes than negatively charged ones (Forest and Pourchez, 2017).

The same good antiviral activity is shown by $HR1_{924-929}$ bound to the positively charged dendrimer when pre-incubated with cells (preventive treatment, setup B). HR1 sequencewas designed to disturb the assembling of 6HB, which is a late event in the fusion mechanism. We can imagine that the peptide bound to the dendrimer is docked on the cell surface. Thus, when the virus is added, the presence of $HR1_{924-929}$ can disturb the proper formation of 6HB and thus fusion and infection. Another possible interpretation of the result is that $HR1_{924-929}$, internalized in the cell thanks to the dendrimer, can interfere with the correct folding of the Spike protein. It is possible that one or the other of the processes occurs or that both are active at the same time. The results obtained show that peptides designed to bind the receptor ACE2 or to interfere with the cell-virus membrane fusion, both key steps for the virus infection, when functionalized with positively charged dendrimers, protect cells to some extent from viral infection. The most successful aspects of our experimental approach may prove useful in the design of peptide-dendrimers to combat other coronaviruses.

Declaration of competing interest

The authors declare that they have no known competing financial interests or personal relationships that could have appeared to influence the work reported in this paper.

Acknowledgements

The authors acknowledge the funding received from Ministerio de ciencia e innovacion PID2020-112924RB-I00, REACT UE-CM2021-01 cofounded by the Community of Madrid (CAM) and the European Union (EU) through the European Regional Development Fund (ERDF) and supported as part of the EU's response to the COVID-19 pandemic Universidad of Alcala: COVID-19 2021 2020/00003/016/001/013, COVID-19 UAH 2019/00003/016/001/004, Regione Campania (POR Campania FESR2014/2020 O.S. 1.3 AZ. 1.3.1 AVVISO DGR 504 del 10/11/2021— CUP B63C22001270002 and CEINGE TASK-FORCE-2022 COVID19 CUP n. D63C22000570002), and Regione Campania (POR Campania FESR 2014/2020, code SURF 21058BP000000020 CUP B63C22001210007).

Appendix A. Supplementary data

Supplementary data to this article can be found online at https://doi.org/10.1016/j.ijpharm.2024.124389.

References

Asl, F.D., Mousazadeh, M., Taji, S., Bahmani, A., Khashayar, P., Azimzadeh, M., Mostafavi, E., 2023. Nano drug-delivery systems for management of AIDS: liposomes, dendrimers, gold and silver nanoparticles. Nanomedicine (Lond.) 18, 279–302.

Barra, T., Falanga, A., Bellavita, R., Laforgia, V., Prisco, M., Galdiero, S., Valiante, S., 2022. gH625-liposomes deliver PACAP through a dynamic in vitro model of the blood-brain barrier. Front. Physiol. 13, 932099.

Bellavita, R., Raucci, F., Merlino, F., Piccolo, M., Ferraro, M.G., Irace, C., Santamaria, R., Iqbal, A.J., Novellino, E., Grieco, P., et al., 2020. Temporin L-derived peptide as a regulator of the acute inflammatory response in zymosan-induced peritonitis. Biomed. Pharmacother. 123, 109788.

Bellavita, R., Falanga, A., Merlino, F., D'Auria, G., Molfetta, N., Saviano, A., Maione, F., Galdiero, U., Catania, M.R., Galdiero, S., et al., 2023. Unveiling the mechanism of action of acylated temporin L analogues against multidrug-resistant Candida albicans. J. Enzyme Inhib. Med. Chem. 38, 36–50.

Breugst, M., Reissig, H.U., 2020. The Huisgen Reaction: Milestones of the 1,3-Dipolar Cycloaddition. Angew. Chem. Int. Ed. Engl. 59, 12293–12307.

Căta, A., Ienașcu, I.M.C., Ștefănuț, M.N., Roșu, D., Pop, O.R., 2023. Properties and Bioapplications of Amphiphilic Janus Dendrimers: A Review. Pharmaceutics 15, 588.

de la Mata, F.J., Gómez, R., Cano, J., Sánchez-Nieves, J., Ortega, P., Gallego, S.G., 2023. Carbosilane dendritic nanostructures, highly versatile platforms for pharmaceutical applications. Wiley Interdiscip. Rev. Nanomed. Nanobiotechnol. 15, e1871.

Del Genio, V., Bellavita, R., Falanga, A., Herve-Aubert, K., Chourpa, I., Galdiero, S., 2022a. Peptides to Overcome the Limitations of Current Anticancer and Antimicrobial Nanotherapies. Pharmaceutics 14, 1235.

Del Genio, V., Falanga, A., Allard-Vannier, E., Herve-Aubert, K., Leone, M., Bellavita, R., Uzbekov, R., Chourpa, I., Galdiero, S., 2022b. Design and Validation of Nanofibers Made of Self-Assembled Peptides to Become Multifunctional Stimuli-Sensitive Nanovectors of Anticancer Drug Doxorubicin. Pharmaceutics 14, 1544.

DeLano, W.L., 2002. The PyMOL Molecular Graphics System. Scientific Research An Academic Publisher.

Eckert, D.M., Malashkevich, V.N., Hong, L.H., Carr, P.A., Kim, P.S., 1999. Inhibiting HIV-1 entry: discovery of D-peptide inhibitors that target the gp41 coiled-coil pocket. Cell 99, 103–115.

Falanga, A., Del Genio, V., Galdiero, S., 2021. Peptides and Dendrimers: How to Combat Viral and Bacterial Infections. In Pharmaceutics 13, 101.

Falanga, A., Maione, A., La Pietra, A., de Alteriis, E., Vitale, S., Bellavita, R., Carotenuto, R., Turra, D., Galdiero, S., Galdiero, E., et al., 2022. Competitiveness during Dual-Species Biofilm Formation of Fusarium oxysporum and Candida albicans and a Novel Treatment Strategy. Pharmaceutics 14, 1167.

Fan, X., Cao, D., Kong, L., Zhang, X., 2020. Cryo-EM analysis of the post-fusion structure of the SARS-CoV spike glycoprotein. Nat. Commun. 11, 3618.

Fernandez, J., Acosta, G., Pulido, D., Malý, M., Copa-Patiño, J.L., Soliveri, J., Royo, M., Gómez, R., Albericio, F., Ortega, P., et al., 2019. Carbosilane Dendron-Peptide Nanoconjugates as Antimicrobial Agents. Mol. Pharm. 16, 2661–2674.

Forest, V., Pourchez, J., 2017. Preferential binding of positive nanoparticles on cell membranes is due to electrostatic interactions: A too simplistic explanation that does not take into account the nanoparticle protein corona. Korean J. Couns. Psychother. 70, 889–896.

Güntert, P., 2004. Automated NMR structure calculation with CYANA. Methods in Molecular Biology (clifton, NJ) 278, 353–378.

Güntert, P., Qiu Qian, Y., Otting, G., Müller, M., Gehring, W., Wüthrich, K., 1991. Structure determination of the Antp(C39 → S) homeodomain from nuclear magnetic resonance data in solution using a novel strategy for the structure calculation with the programs DIANA, CALIBA, HABAS and GLOMSA. J. Mol. Biol. 217, 531–540.

Hernando-Gozalo, M., Aguilera-Correa, J.J., Rescalvo-Casas, C., Seijas-Pereda, L., García-Bertolín, C., de la Mata, F.J., Sánchez-Nieves, J., Cuadros, J., Pérez-Tanoira, R., 2023. Study of the antimicrobial activity of cationic carbosilane dendrimers against clinical strains of multidrug-resistant bacteria and their biofilms. Front Cell Infect Mi 13, 1203991.

Jackson, C.B., Farzan, M., Chen, B., Choe, H., 2022. Mechanisms of SARS-CoV-2 entry into cells. Nature reviews Molecular cell biology 23, 3–20.

Koradi, R., Billeter, M., Wüthrich, K., 1996. MOLMOL: a program for display and analysis of macromolecular structures. Journal of molecular graphics 14 (51–55), 29–32.

Lan, J., Ge, J., Yu, J., Shan, S., Zhou, H., Fan, S., Zhang, Q., Shi, X., Wang, Q., Zhang, L., et al., 2020. Structure of the SARS-CoV-2 spike receptor-binding domain bound to the ACE2 receptor. Nature 581, 215–220.

Li, W., Zhang, C., Sui, J., Kuhn, J.H., Moore, M.J., Luo, S., Wong, S.K., Huang, I.C., Xu, K., Vasilieva, N., et al., 2005. Receptor and viral determinants of SARS-coronavirus adaptation to human ACE2. EMBO J. 24, 1634–1643.

Maroun, R.G., Krebs, D., El Antri, S., Deroussent, A., Lescot, E., Troalen, F., Porumb, H., Goldberg, M.E., Fermandjian, S., 1999. Self-association and domains of interactions of an amphipathic helix peptide inhibitor of HIV-1 integrase assessed by analytical ultracentrifugation and NMR experiments in trifluoroethanol/HO mixtures. J. Biol. Chem. 274, 34174–34185.

Murdocca, M., Citro, G., Romeo, I., Lupia, A., Miersch, S., Amadio, B., Bonomo, A., Rossi, A., Sidhu, S.S., Pandolfi, P.P., et al., 2021. Peptide Platform as a Powerful Tool in the Fight against COVID-19. Viruses 13, 1667.

Passariello, M., Esposito, S., Manna, L., Rapuano Lembo, R., Zollo, I., Sasso, E., Amato, F., De Lorenzo, C., 2023. Comparative Analysis of a Human Neutralizing mAb Specific for SARS-CoV-2 Spike-RBD with Cilgavimab and Tixagevimab for the Efficacy on the Omicron Variant in Neutralizing and Detection Assays. In. Int. J. Mol. Sci. 10053.

Pettersen, E.F., Goddard, T.D., Huang, C.C., Couch, G.S., Greenblatt, D.M., Meng, E.C., Ferrin, T.E., 2004. UCSF Chimera–a visualization system for exploratory research and analysis. J. Comput. Chem. 25, 1605–1612.

Ravasco, J., Faustino, H., Trindade, A., Gois, P.M.P., 2019. Bioconjugation with Maleimides: A Useful Tool for Chemical Biology. Chemistry (weinheim an Der Bergstrasse, Germany) 25, 43–59.

Shang, J., Ye, G., Shi, K., Wan, Y., Luo, C., Aihara, H., Geng, Q., Auerbach, A., Li, F., 2020. Structural basis of receptor recognition by SARS-CoV-2. Nature 581, 221–224.

Sherje, A.P., Jadhav, M., Dravyakar, B.R., Kadam, D., 2018. Dendrimers: A versatile nanocarrier for drug delivery and targeting. Int. J. Pharm. 548, 707–720.

Sun, H., Li, Y., Liu, P., Qiao, C., Wang, X., Wu, L., Liu, K., Hu, Y., Su, C., Tan, S., et al., 2020. Structural basis of HCoV-19 fusion core and an effective inhibition peptide against virus entry. Emerging Microbes Infect. 9, 1238–1241.

Walls, A.C., Park, Y.J., Tortorici, M.A., Wall, A., McGuire, A.T., Veesler, D., 2020. Structure, Function, and Antigenicity of the SARS-CoV-2 Spike Glycoprotein. Cell 181, 281–292.e286.

Wang, Q., Zhang, Y., Wu, L., Niu, S., Song, C., Zhang, Z., Lu, G., Qiao, C., Hu, Y., Yuen, K. Y., et al., 2020. Structural and Functional Basis of SARS-CoV-2 Entry by Using Human ACE2. Cell 181, 894–904.e899.

Wishart, D.S., Sykes, B.D., Richards, F.M., 1992. The chemical shift index: a fast and simple method for the assignment of protein secondary structure through NMR spectroscopy. Biochemistry 31, 1647–1651.
Wüthrich, K., 1986. NMR of Proteins and Nucleic Acids. Wiley, New York, p. 320.
Yousif, A.M., Ingangi, V., Merlino, F., Brancaccio, D., Minopoli, M., Bellavita, R., Novellino, E., Carriero, M.V., Carotenuto, A., Grieco, P., 2018. Urokinase receptor derived peptides as potent inhibitors of the formyl peptide receptor type 1-triggered cell migration. Eur. J. Med. Chem. 143, 348–360.
Zhang, J., Cai, Y., Xiao, T., Lu, J., Peng, H., Sterling, S.M., Walsh, R.M., Rits-Volloch, S., Sliz, P., Chen, B., 2020. Structural Impact on SARS-CoV-2 Spike Protein by D614G Substitution. 372, 525–530 bioRxiv : the preprint server for biology.